Graphene Based Wideband Electromagnetic Absorbing Textiles at Microwave Bands

Alessandro Giuseppe D'Aloia, *Member, IEEE*, Hossein Cheraghi Bidsorkhi, *Member, IEEE*, Giovanni De Bellis, *Member, IEEE*, and Maria Sabrina Sarto, *Fellow, IEEE*

***Abstract*—The design and realization of graphene based wideband electromagnetic (EM) absorbing textiles are becoming of primary interest. Hence, the development of new conductive coatings to be cast onto commercial textiles is crucial. In this article, we propose new graphene based absorbing textiles that conjugate outstanding EM absorbing properties at radiofrequency with low-weight, flexibility, cost-effectiveness, and washability. With this purpose, an innovative production process of polyvinylidene fluoride (PVDF) coatings filled with graphene nanoplatelets (GNPs) is developed for the production of radar-absorbing coated textiles, which are fully characterized in terms of morphological, electrical, and EM absorbing properties. In particular, the complex dielectric permittivity of the coated textiles including different amounts of GNPs is assessed through the measurement of the complex permittivity of a benchmark sample, the consequent estimation of the average GNP size and the prediction by simulations of the effective complex permittivity of graphene based coatings loaded with different GNP amounts. Such predicted data are crucial to design radar absorbing textiles with minimum bandwidths at −10 dB of 5 GHz and reflection coefficients below −5 dB over all the frequency range from 8 up to 18 GHz. These textiles are then produced and characterized in terms of reflection coefficient in free space against a plane wave with normal incidence. The obtained results demonstrate the full satisfaction of the design requirements. In fact, the produced samples show a reflection coefficient with a bandwidth at −10 dB up to 77% of the resonant frequency.**

***Index Terms*—Graphene based composites, graphene nanoplatelets (GNPs), polyvinylidene fluoride (PVDF), radar absorbing materials.**

I. Introduction

THE wide-spreading development of electronic devices based on densely packed integrated circuits along with telecommunication systems has significantly increased electromagnetic (EM) interference issues [1]. As a consequence, nowadays EM pollution is a major concern that could seriously compromise equipment performance and electronic basic functions, leading to lifetime reduction and loss of energy and data degradation in signals and storage devices [2]. For instance, undesired EM radiation can be deleterious to aviation safety by interfering with air traffic control systems and affecting the signal quality in communication devices [3]–[5]. Hence, EM absorption is becoming of primary interest and the development of new absorbers is currently one of the major research topics.

In fact, EM wave absorption is crucial for several applications, including industrial and commercial ones, satellite communication, spacecraft, and stealth technology [6]. As an example, satellite communication systems consist of transmitter and receiver antennas that operate on different frequency ranges. To avoid EM interferences, absorbers are commonly used [7]–[9], leading to signal noise reduction and signal quality improvement [3]. Additionally, EM absorbers play a key role in defense applications, being used for stealth and camouflage applications, such as the reduction of the radar signature of ships, tanks, and aircrafts [10], [11].

As a consequence, weight reduction is crucial and EM absorption capabilities, combined with good chemical, mechanical, and thermal properties, are believed to be key requirements in forthcoming flexible and miniaturized electronic devices [11], which are being increasingly considered for applications involving human–machine and device-to-device interactions, such as those related to wearable technology. Traditional absorbing materials, such as magnetic metal powders [12], ferrite [13], and ceramics [14], have a limited use in emerging electronic and communication technologies due to their high density, heavy weight, and susceptibility to environmental degradation [15], [16].

In light of the foregoing, it is believed that exploring radar absorbing materials in wearable technology will open up many applications related to EM absorption [16]–[19]. A multitude of textile materials, such as felts, yarns, woven, or nonwoven fabrics, are already being investigated, and many different approaches are being developed to make commercial textiles suitable for EM radar absorption [20]. While recent studies have shown the possibility to combine metallic particles with textiles to improve their EMI shielding properties, such fillers can give rise to several issues, like oxidation, corrosion, weight increase, or processing difficulties [19]–[21]. To solve these problems, conductive polymeric materials, either based on intrinsically conductive polymers or on insulating matrices loaded with

Manuscript received December 21, 2020; revised June 21, 2021 and November 16, 2021; accepted December 4, 2021. Date of publication January 10, 2022; date of current version June 13, 2022. This work was partially supported by Soliani EMC who provided also plain textiles. *(Corresponding author: Alessandro Giuseppe D'Aloia.)*

The authors are with the Department of Astronautical, Electrical and Energy Engineering of Sapienza University of Rome, 00184 Roma, Italy, and also with the Research Center for Nanotechnology applied to Engineering of Sapienza University, 00185 Roma, Italy (e-mail: alessandrogiuseppe.daloia@uniroma1.it; hossein.cheraghibidsorkhi@uniroma1.it; giovanni.debellis@uniroma1.it; mariasabrina.sarto@uniroma1.it).

Color versions of one or more figures in this article are available at https://doi.org/10.1109/TEMC.2021.3133665.

Digital Object Identifier 10.1109/TEMC.2021.3133665

This work is licensed under a Creative Commons Attribution-NonCommercial-NoDerivatives 4.0 License. For more information, see https://creativecommons.org/licenses/by-nc-nd/4.0/

conducting fillers, have been also considered in recent literature [20]–[25].

In particular, polymeric coatings can be applied to the surface of fabrics, yarns or felts, avoiding the direct exposure of textiles to damaging oxidizing agents and fulfilling the requirements for controlled laboratory conditions [20]–[22]. However, despite the benefits of conductive polymer coatings, their practical realization is still a challenging task [16]. In fact, due to strong interaction within polymer chains, polymers are often insoluble in common solvents and might result hard to melt. Hence, they are difficult to spin to produce filaments or fibers. Moreover, lack of thermal stability makes them unsuitable for casting onto textiles [20] and they can be easily peeled off the textile during processing and use [23]. Also, cleaning conductive polymer-coated textiles can be likewise problematic because, after washing, polymers might undergo a degradation of some of their properties, such as electrical conductivity [16], [20].

On the other hand, graphene based nanocomposite coatings can present several advantages over commonly employed conductive coatings and their study and development is still attracting a great deal of attention [16], [20], [21]. Graphene represents a whole new class of two-dimensional (2-D) carbon nanostructure and possesses, not only a stable structure, but also a high specific surface area, combined with excellent electrical properties. Such qualities are crucial for the realization of nanocomposites with outstanding mechanical, thermal, electrical, and EM properties [17]–[24].

Moreover, being cost-effective and having a high specific surface area and low density, these nanocomposites constitute one of the most promising materials to significantly reduce the weight of EM absorbing materials [25], [26]. However, despite extensive research efforts, the production of graphene-based coatings for the realization of EM absorbing textiles is still an open issue due to problems in coating's adhesion, properties' loss during washing cycles, more delicate handling needs of coated textiles over uncoated ones [20].

The aim of this work is to overcome these bottlenecks, producing a cost-effective light-weight graphene-based coating for wideband EM wave absorption, to be cast directly onto commercial textiles.

With this purpose, polyvinylidene fluoride (PVDF) is selected as the polymer matrix and graphene nanoplatelets (GNPs) are chosen as graphene-based nanofillers. The choice of PVDF has been driven by its high chemical and thermal resistances and its wide employment in industrial applications [27]. Moreover, it is proved that graphene-based PVDF composites possess good EM wave absorption properties [28], [29]. In addition, they show strong hydrophobicity [30], making them washable several times without properties degradation [31].

GNPs are small stacks of graphene layers that are 1 to 10 nm thick, with lateral dimensions up to 10 μm [32]. They gained most attention as nanofillers in polymer composites, since they are extremely cheap, easily processable and characterized by outstanding mechanical properties, along with high thermal and electrical conductivities [17]. In addition, several GNP-filled composites have been developed and their application as conductive coatings and microwave absorbers, for frequencies up to 18 GHz, has been largely demonstrated [17], [24]–[29], [31]–[33].

In this article, different PVDF/GNP nanocomposite coatings are produced and cast onto different commercial polyester textiles, specifically a felt and a woven fabric, producing graphene based wideband EM absorbing textiles. The coatings are morphologically and physically characterized through scanning electron microscopy (SEM) and atomic force microscopy (AFM) analyses. In addition, in order to gain a preliminary indicator of their resistance to washing cycles, the wettability of the coated textiles is assessed through water contact angle (CA) measurements. In fact, it is demonstrated that super-hydrophobic surfaces, i.e., the ones characterized by a CA greater than 150°, are capable of resisting long-term real world exposure and industrial contamination tests [31]. This feature could be particularly interesting for all-weather outdoor electronic equipment, such as signal stations, since they raise new expectations for additional features, like strong corrosion resistance and self-cleaning capabilities [16], [35], [36].

The EM properties of the PVDF/GNP coatings are assessed through an innovative technique. The effective complex dielectric permittivity of a benchmark PVDF/GNP coating over a Rohacell (RC) substrate is measured and the results are used to estimate the average dimensions of GNPs in the coating, allowing the prediction by simulations of the effective complex permittivity of graphene-based coatings loaded with different GNP amounts. The estimated GNPs' average dimensions are validated by comparison with both AFM and SEM analyses and then used to design radar absorbing coatings in order to realize wideband EM absorbing textiles with minimum bandwidths at -10 dB wider than 5 GHz and reflection coefficients below -5 dB over the entire frequency range from 8 up to 18 GHz. This reflection coefficient values have been taken as a reference in order to compare the EM wave absorption of the produced graphene-based absorbing textiles with commercially available flexible polymeric absorbers.

Finally, the predicted reflection coefficients are compared with the measured ones. It is noticed a good agreement between the computed and measured results and all the produced graphene-based absorbing textiles satisfy the EM design requirements, showing bandwidths at -10 dB ranging between 40% and 77% of the resonant frequency.

II. Materials and Method

A. Fabrication of Graphene Based EM Absorbing Textiles

Commercially available graphite intercalation compounds (GIC) are subjected to a thermal shock, obtaining worm-like expanded graphite (WEG), which is subsequently sonicated to obtain GNPs, as described in [37]. Following the GIC thermal expansion, leading to WEG, PVDF is dissolved in N,N-dimethylformamide (DMF), through 2 h magnetic stirring at 65°C. Successively, WEG is added to the PVDF–DMF solution and the obtained dispersion is tip sonicated using an ultrasonic processor, thus leading to a homogeneous suspension of GNPs in a PVDF–DMF solution. The GNP weight concentrations with respect to the PVDF amount are 9% wt, 10% wt, and 13% wt.

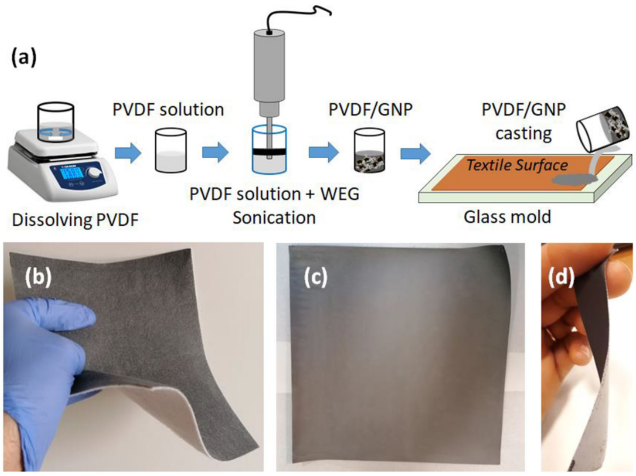

Fig. 1. (a) PVDF-Graphene coating fabrication route and (b) resulting PVDF/GNP coated felt and (c), (d) PVDF/GNP coated fabrics.

Finally, the PVDF–DMF–GNP mixture is cast on a commercial polyester textile and rapidly placed into an oven to get rid of the residual solvent. Two commercial textiles are considered: a felt and a fabric, both made of polyester and shaped to form a 30 cm $\times$ 30 cm square. The felt has a porosity greater than 99% and therefore a relative dielectric permittivity almost equal to one. On the other hand, the relative dielectric permittivity of the polyester fabric is equal to 1.7 [38].

The production process is sketched in Fig. 1(a), while Fig. 1(b)–(d) shows PVDF/GNP coatings on the felt and on the woven fabric, respectively. Both PVDF/GNP coatings are uniform and homogeneous and the coated textiles are low-weight and they can be handled easily, without the risk of damaging the conductive coating.

B. Morphological and Physical Characterization

The morphology of PVDF/GNP coatings is analyzed using a Zeiss Auriga high-resolution SEM available at Sapienza Nanotechnology and Nanoscience Laboratory (SNN-Lab) of Sapienza University of Rome.

The composite samples are fractured in liquid nitrogen and coated with $\sim$20 nm-Cr using a Quorumtech Q150T sputter coater, in order to prevent charging.

Successively, AFM analysis is carried out by using a Bruker Dimension Icon AFM. The specimen employed for the analysis is obtained by drop-casting a GNPs dispersion in acetone onto the polished side of a silicon wafer chip. AFM micrographs are acquired in tapping mode, over a scanning area of 5 μm $\times$ 5 μm. SEM images are analyzed and elaborated using the Mountains Map 7 software.

Finally, hydrophobicity is assessed through the measurement of water CAs. Such measurements are carried out by using an optical CA meter available at SNN-Lab and casting $\sim$2 μl water droplets on the coating surface.

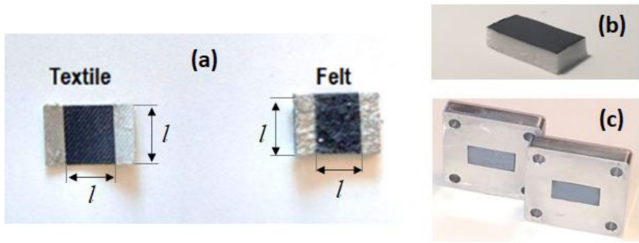

Fig. 2. (a) Textile coated with PVDF/GNP nanocomposite, (b) PVDF/GNP coating over *RC* substrate and (c) inserted in Ku-band flanges for EM characterization.

C. DC Electrical Characterization

The produced PVDF/GNP coatings are electrically characterized via the measurement of the sheet resistances $R_{\rm s}$. With this purpose, the coated textiles are cut into rectangular samples and the opposite sides of each rectangular specimen are coated with silver conductive paint (Electrolube), providing two rectangular contacts, as shown in Fig. 2(a). Then, tin-coated copper wires are bonded to the aforementioned contact pads using a bi-component Ag-filled epoxy adhesive (Circuitworks). Subsequently, the samples are cured in oven at 120°C for 10 min. The produced samples are electrically characterized applying the two-wire volt-amperometric method using a Keithley 6221 dc/ac current source connected to a Keithley 2182a nano-voltmeter, controlled by a laptop.

Since the surface between the silver electrical contacts is a square of side l [see Fig. 2(a)], the effective dc electrical conductivity of each sample $\sigma_{\rm dc}$ is extracted from the measured sheet resistance value $R_{\rm S}$ as

$$\sigma_{\rm dc} = (tR_{\rm S})^{-1} \tag{1}$$

where t is the coating thickness of the produced PVDF/GNP coatings. In this regard, it is worth to notice that the selected textiles do not contribute to electrical conduction since they are made of polyester, a nonconducting material.

For each coating type three measurements are acquired and results are averaged, in order to avoid errors due to local filler agglomeration and surface inhomogeneities.

D. EM Characterization

At first, benchmark samples are produced. To this purpose, a homogeneous suspension of 9% wt GNPs in PVDF-DMF solution is cast onto commercial *RC* panels. Then, instead of being placed into an oven, the *RC* panels are rapidly immersed into a water coagulation bath at room temperature upon phase inversion completion, with the aim of removing DMF [39].

Successively, the samples are dried at room temperature, cut to the desired shape and inserted inside Ku-band flanges, as shown in Fig. 2(b) and (c).

Finally, the scattering parameters of the graphene-based coatings over the *RC* substrates are measured using a vector network analyzer (Anritsu Vector Star 239 MS4647A) and the Ku-band waveguide, in order to cover the 12.4–18 GHz frequency range.

The complex effective permittivity of the PVDF/GNP coatings is then obtained applying the cascade de-embedding method described in [40] and assuming a dielectric permittivity of 1.08 for the employed *RC* substrate

E. Average Size Estimation of GNPs and EM Modeling of PVDF/GNP Coatings

The average size of GNPs is estimated through the analysis of the complex effective permittivity measurements of benchmark samples. In particular, these samples are modeled using the multiscale Maxwell Garnett (MG) formula [28], since this model permits to take into account the 2-D irregular shape of GNPs [33]. It is worth to notice that traditional MG formula and other models available in the literature generally assume that the filler has an ellipsoidal shape [28], [33], [41]. As a consequence, the effects of EM field scattering, localizations, and enhancements due to GNPs shapes cannot be properly taken into consideration [37]. In order to overcome this limitation and to consider the interaction between the filler and the polymeric matrix at both nano- and microscales [32], [33], the PVDF/GNP coatings are modeled as effective two-filler composites, where the first filler is constituted by oblate ellipsoids, and the second is represented by nanorods. The first filler mainly affects the dielectric permittivity of the nanocomposite while the second affects principally the conducting properties of the material. Therefore, MG formula is applied recursively.

At first, the effective permittivity of the polymeric matrix filled with oblate ellipsoids having axes $l_{\rm GNP}$ and $t_{\rm GNP}$ equal to the average GNPs lateral dimension and thickness is computed as

$$\varepsilon_{obl} = \varepsilon_m + \frac{\varepsilon_m \theta_{GNP}\left(1-\varepsilon_m - j\sigma_{GNP}/\omega\varepsilon_0\right)\sum_{k=1}^{3}\Lambda_k}{3-\theta_{GNP}\left(1-\varepsilon_m - j\sigma_{GNP}/\omega\varepsilon_0\right)\sum_{k=1}^{3}\Gamma_k} \tag{2}$$

with

$$\Lambda_k = \frac{1}{\varepsilon_m + N_{kobl}\left(1-\varepsilon_m - j\sigma_{GNP}/\omega\varepsilon_0\right)} k=1,3 \tag{3a}$$

$$\Gamma_k = \frac{N_{kobl}}{\varepsilon_m + N_{kobl}\left(1-\varepsilon_m - j\sigma_{GNP}/\omega\varepsilon_0\right)} k=1,3 \tag{3b}$$

where $\varepsilon_{\rm m}$ is the relative dielectric constant of the matrix, $\theta_{\rm GNP}$ is the GNP volume fraction, and $N_{k\rm obl}$ (k = 1,3) are the oblate depolarization factors defined in [37]. The electrical conductivity $\sigma_{\rm GNP}$ is set equal to 10.5 kS/m, i.e., to the average value of highly dense GNP films produced and electrically characterized in [37].

Successively, the MG expression is applied considering that rod-shaped inclusions are dispersed in the effective medium constituted by the matrix loaded with the oblate ellipsoids having effective permittivity $\varepsilon_{\rm obl}$. It yields

$$\varepsilon = \varepsilon_{obl} + \frac{\varepsilon_{obl}\alpha\theta_{GNP}\left(1-j\sigma_{GNP}/\omega\varepsilon_0 - \varepsilon_{obl}\right)\sum_{k=1}^{3}\Pi_k}{3-\alpha\theta_{GNP}\left(1-j\beta\sigma_{GNP}/\omega\varepsilon_0 - \varepsilon_{obl}\right)\sum_{k=1}^{3}\Psi_k} \tag{4}$$

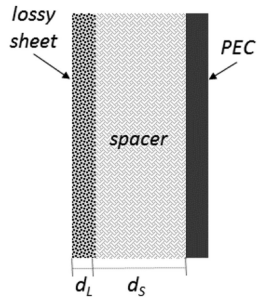

Fig. 3. Basic configuration of a Salisbury absorbing screen.

with

$$\Pi_k = \frac{1}{\varepsilon_{\rm m} + N_{k\rm rod}\left(1-\varepsilon_{\rm m} - j\beta\sigma_{GNP}/\omega\varepsilon_0\right)} k=1,3 \tag{5a}$$

$$\Psi_k = \frac{N_{k\rm rod}}{\varepsilon_{\rm m} + N_{k\rm rod}\left(1-\varepsilon_{\rm m} - j\beta\sigma_{GNP}/\omega\varepsilon_0\right)} k=1,3 \tag{5b}$$

where $\varepsilon = \varepsilon' + j\varepsilon''$ is the relative complex permittivity of the coating and $N_{k\rm rod}$ are the depolarization factors of the rod shaped fillers [37] having dimensions $l_{\rm rod} = \gamma\, l_{\rm GNP}$ and $t_{\rm rod} = t_{\rm GNP}$. Notice that $l_{\rm rod}$ is representative of the average linear extension of the GNP folds and is proportional to the average GNPs lateral dimension through the constant γ [33]. On the other hand, α and β are parameters dependent upon the GNP dispersion degree in the polymeric matrix [32].

The numerical fitting of the measured complex dielectric permittivity through the use of the MG model can thus provide an estimate of the average size of the filler dimensions in the produced composite coatings [41]. The reliability of such estimations is verified through comparison with morphological characterizations of the composite, specifically with SEM and AFM images, performed on both the benchmark sample and on coated textiles.

Once the average dimension of the GNPs in the PVDF/GNP coatings has been estimated, the complex effective permittivity of the produced nanocomposite coatings is predicted by means of the MG model [37]. The main advantage of this method relies on the fact that only a few benchmark samples are needed to predict the EM characteristics of different coatings filled with various GNP amounts.

F. Theory of Absorbing Screens and Modeling

The most common absorbing screen is the Salisbury one, whose basic structure is sketched in Fig. 3. Briefly, the first layer from the left side is the lossy sheet, and its function is to absorb the EM energy associated with the incident field. The second layer is the spacer, which is generally made of a lossless dielectric material backed by a thick metal slab, realizing a perfect electric conducting (PEC) plate, whose function is to reflect all the energy associated to the incident field [42]. The lossy sheet and the spacer have thicknesses $d_{\rm L}$ and $d_{\rm S}$, respectively.

The lossy sheet is characterized by its effective complex relative permittivity $\varepsilon_{\rm L} = \varepsilon'_{\rm L} + j\varepsilon''_{\rm L}$, where $\varepsilon'_{\rm L}$ is the relative

effective dielectric constant, and $\varepsilon''_{\mathrm{L}}$ is the lossy term. The absolute value of $\varepsilon''_{\mathrm{L}}$ is related to the effective electrical conductivity σ_{L} of the lossy sheet, according to

$$\sigma_L = \omega\varepsilon_0 \left|\varepsilon''_L\right|. \tag{6}$$

The spacer is assumed to be lossless and characterized by real relative permittivity ε_{S}.

The absorber reflection coefficient *R* is defined as the ratio between the amplitudes of the reflected and of the incident electric fields [42].

According to the transmission line formalism, it can be expressed as

$$R = 20\log_{10}\left|\frac{Z_{\mathrm{in}} - \eta_0}{Z_{\mathrm{in}} + \eta_0}\right|, \tag{7}$$

where η_0 is the free space impedance and Z_{in} the overall input impedance, given by

$$Z_{\mathrm{in}} = \frac{\Phi_{12}}{\Phi_{22}} \tag{8}$$

being Φ_{22} and Φ_{12}, the coefficients of the overall output-to-input transmission matrix [32].

The classical theory of Salisbury screens is based on the hypothesis that the lossy sheet is electrically thin and purely resistive and the spacer is lossless and non-dispersive, with thickness d_{S} equal to $\lambda_{\mathrm{S}}/4$, λ_{S} being the wavelength of the EM field in the spacer at the frequency f_{r} of minimum reflection

$$f_r = \frac{c_0}{4d_S\sqrt{\varepsilon_S}}. \tag{9}$$

At the frequency f_{r} and under the aforementioned hypothesis, the overall input impedance assumes the following form:

$$Z_{\mathrm{in}}(f_r) = (\sigma_{\mathrm{L}} d_{\mathrm{L}})^{-1}. \tag{10}$$

Combining (7) and (10), the condition for minimum reflection at the frequency f_{r} reads [39]

$$\sigma_L d_L = 1/\eta_0. \tag{11}$$

This condition represents a real bottleneck in the design of absorbers, since it constrains the total thickness of the screen.

In order to overcome such constraint, the lossy sheet can be made of a dispersive material with tailored effective complex permittivity, contributing to the reduction of the overall thickness absorber [24], [33]. The minimum reflection coefficient at the frequency f_{r} is then obtained through numerical iterations by minimizing (7), with Z_{in0} given by (8) [32]. The resulting spacer's thickness is thinner than $\lambda_{\mathrm{S}}/4$, as discussed in [32].

G. Reflection Coefficient Measurement

The reflection coefficients of the produced absorbing textiles are measured in the frequency range from 6 GHz up to 18 GHz. The produced graphene coated textiles have dimensions of 30 cm × 30 cm and are located at the Fraunhofer distance (far field) from a pair of properly designed wide-band horn antennas [29].

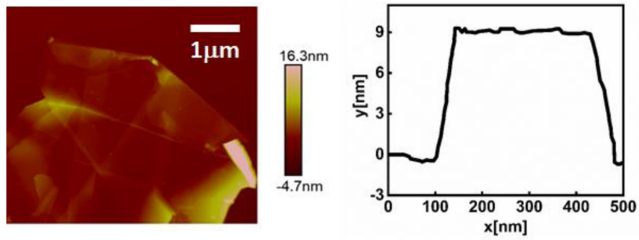

(a) (b)

Fig. 4. (a) AFM image of a GNP and (b) corresponding thickness profile.

The measurements are performed for normal incidence by using an Anritsu Vector Star MS4647A vector network analyzer available at Sapienza University of Rome.

III. Results and Discussions

A. Morphological, Chemical, and Physical Characterization

Fig. 4(a) shows an AFM height signal map of a GNP placed on a silicon wafer. It is noticed that GNPs have an irregular 2-D shape, with sharp edges and wrinkles, lateral dimensions in the micrometer range and vertical dimensions in the order of few nanometers. In particular, when looking at the height profile reported in Fig. 4(b), it can be noticed that the analyzed GNP has a thickness around 9 nm.

False-colored SEM images of the produced PVDF/GNP coatings over a *RC* panel and over a polyester fabric are reported in Fig. 5. In particular, the PVDF/GNP coating over a *RC* panel is loaded at 9% wt, while the coating over the woven fabric is filled with 10% wt GNPs.

Fig. 5(a) and (b) shows the surfaces of an uncoated *RC* and a commercial polyester fabric, respectively, both colored in light blue. The *RC*, used for the production of benchmark samples, has a surface characterized by a tetrakaidecahedron geometry with adjacent hexagonal and squared cells having dimensions in the micrometer range. On the other hand, the polyester fabric surface micrograph shows oriented woven fibers composing the virgin textile structure.

Looking at Fig. 5(c) and (d), showing the top surfaces of PVDF/GNP coated *RC* and fabric, respectively, it is possible to notice that both surfaces are completely covered by a continuous, uniform, and homogeneous PVDF/GNP composite coating, plum colored in Fig. 5(e), and (f). In fact, neither the *RC* nor the fabric substrates are visible in the SEM images.

Then, Fig. 5(e), (f) and (g), (h) report the SEM cross-sections of the PVDF/GNP coating over *RC* and commercial fabric, respectively, at different magnifications. It is clear that the PVDF/GNP coatings are thoroughly embedded in the *RC* and fabric surfaces. Moreover, Fig. 5(g) and (h), highlight a very good adhesion of GNPs to the PVDF polymer matrix through functional links, as observed also in previous works [24], [27]. For the sake of clarity, the substrates and the polymer matrices are colored in light blue and in red, respectively, while the GNPs are highlighted in yellow.

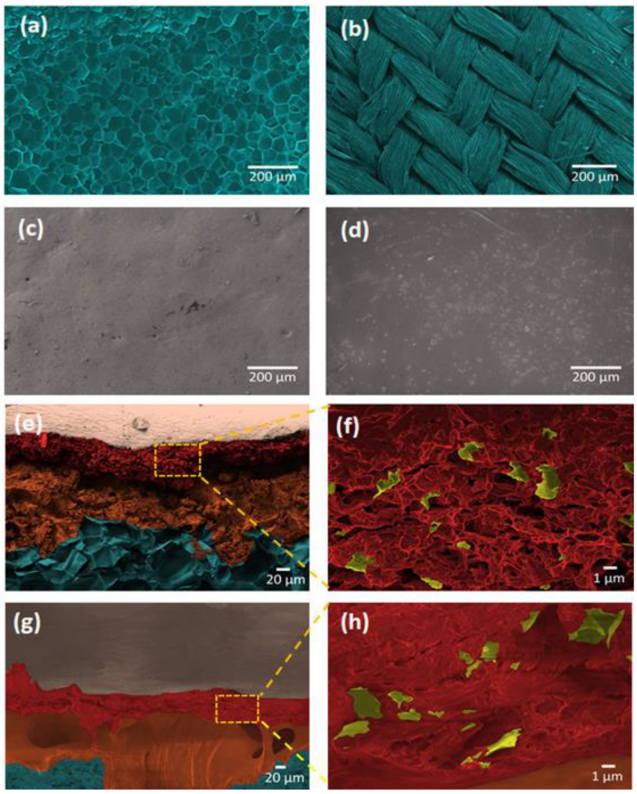

Fig. 5. SEM micrographs of representative samples. (a), (b) Surfaces of an uncoated *RC* and a commercial polyester fabric, respectively. (c), (d) PVDF/GNP coated surfaces of a *RC* and a fabric, respectively. (e), (f) PVDF/GNP coating over *RC* at different magnifications. (g), (h) PVDF/GNP coating over polyester fabric at different magnifications.

Finally, comparing Fig. 5(f) and (h), it can be noticed that GNPs show similar average lateral size, even though these images refer to coatings cast on different substrates and loaded with different GNP concentrations. This observation is a confirmation that we can predict the EM characteristics of PVDF/GNP coatings through average size estimation of GNPs in the benchmark samples and through the use of the MG model, as described in Section II.

Finally, the wettability properties of the produced PVDF/GNP coated fabric and *RC* are assessed through the water CA measurement, performed before and after deposition of the PVDF/GNP coating over the *RC* and polyester fabric substrates.

As shown in Fig. 6(a) and (b), the CAs on the uncoated *RC* and on the commercial fabric are respectively equal to 93°± 3 and 51°± 3. Thus, we conclude that *RC* substrate is slightly hydrophobic while the polyester fabric, selected for the realization of graphene based absorber textiles, is hydrophilic.

When both substrates are coated with PVDF/GNP composite loaded at 9% wt, we notice that the CA rises sharply, reaching values as high as 159°± 3 in the case of the *RC* substrate [see Fig. 6(c)] and 153°± 3 in the case of the coated polyester fabric [see Fig. 6(d)]. In fact, in both cases water droplets form an almost complete circular shape, showing hydrophobicity, even though, before being coated, the polyester fabric was hydrophilic.

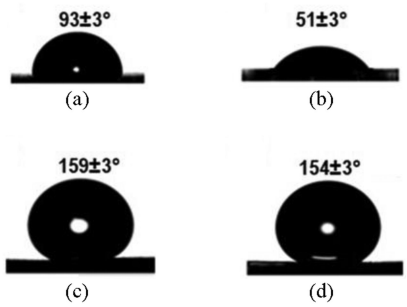

Fig. 6. CA images of Rohacell and commercial polyester fabric (a), (b) before coating and (c), (d) after coating.

TABLE I
SHEET RESISTANCE AND DC ELECTRICAL CONDUCTIVITY OF THE PRODUCED PVDF/GNP COATED TEXTILES

GNP concentration [% wt.]	Textile	R_s [Ω/□]	t [μm]	σ_{dc} [S/m]
10	felt	791	70	18
10	felt	804	60	21
13	fabric	552	60	30.2

Therefore, the PVDF/GNP coating makes the coated surface superhydrophobic, regardless of substrate type. Hence, graphene based coatings provide extensive features to the produced absorbing textiles such as moisture resistance, self-cleaning, and water-proof capabilities [35], [36]. These properties are of great interest for the design of new absorbers [16], capable of resisting long-term real world exposure and industrial contamination tests [36].

B. DC Electrical Conductivity

The produced PVDF/GNP coatings filled with 10% wt and 13% wt GNPs are electrically characterized as described in the Experimental Section. Table I reports the average values of the measured sheet resistances R_s of PVDF/GNP coatings cast over felt or fabric textile. Then, the electrical conductivity σ_{dc} is computed by means of (1).

It is noticed that σ_{dc} depends principally on GNPs' concentration, increasing when more GNPs are added to the polymer matrix. Moreover, the conductivity of coatings cast over felt, both loaded at 10% wt. but having different thickness values t, are slightly different, indicating that the GNP dispersion is affected by the coating thickness. In fact, the thicker coating has a lower conductivity with respect to the thinner one. This difference is due to filler's agglomeration and disuniformitiy formed during the casting process [41].

C. EM Characterization

Fig. 7(a) shows the frequency spectra of the real ε' and imaginary ε'' parts of the effective relative complex permittivity ε of the produced PVDF/GNP nanocomposite coatings while Fig. 7(b) shows the ac effective electrical conductivity σ_{ac}, evaluated by means of (6), replacing $\varepsilon_L{}''$ with ε''.

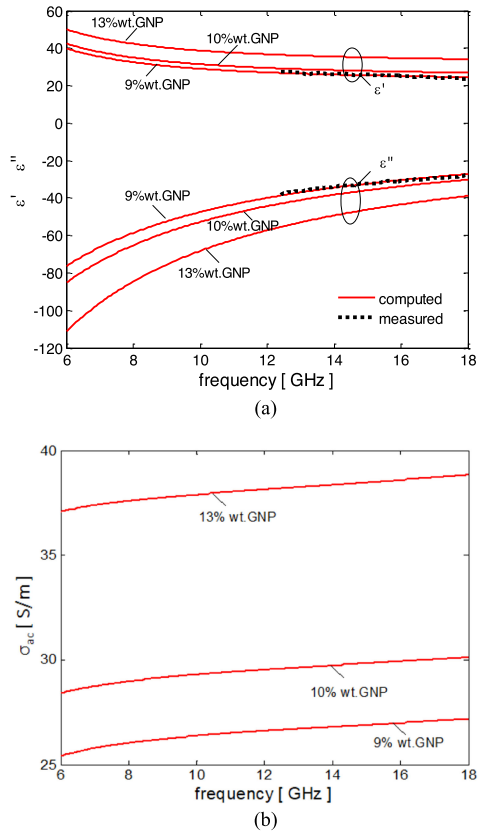

Fig. 7. (a) Frequency spectra of the real part and imaginary part of the effective complex permittivity and (b) of the ac electrical conductivity of the produced PVDF-graphene nanocomposite coatings filled with GNPs at 9% wt, 10% wt, and 13% wt.

The measured real and imaginary parts of the dielectric permittivities of the benchmark sample are reported in Fig. 7(a) using dashed black lines in the 12–18 GHz frequency range. In the same figure, the solid red lines indicate the predicted real and imaginary parts of the dielectric permittivities of the PVDF/GNP coatings over textiles.

Through numerical fitting of measured data, we estimated that GNPs have average thickness around 9 nm and average lateral dimension of 5 μm. Such estimations, obtained following the procedure described in [41], are confirmed by AFM and SEM images, performed on coatings cast over different substrates and having different GNP amount, as explained in Section III. Hence, these estimations are used to predict the complex permittivities of the produced PVDF/GNP coatings over textiles in the 6–18 GHz frequency range by means of the MG model [41].

As a further confirmation of the reliability of the GNP size estimations and of the use of MG model, we notice that the predicted real and imaginary parts of the dielectric permittivity of the benchmark sample, computed in the frequency range from 6–18 GHz, are almost overlapping with experimental data, measured from 12.4 up to 18 GHz.

Then, we point out that the lossy properties of the coatings are demonstrated by the high values of $|\varepsilon''|$ and $\sigma_{\rm ac}$ in the considered frequency range. Moreover, the ac electrical conductivity increases with GNPs' concentration, as already observed in the dc electrical conductivity characterization.

Finally, we notice that the ac electrical conductivity of the coatings increases very slightly with frequency, whereas the real part of the effective permittivity decreases. As discussed in [32], this behavior enables wide-band absorption capabilities over the considered frequency range.

D. Design of Graphene Based Absorbing Textiles

The final goal of the study is the realization of graphene based wideband EM absorbing textiles, with bandwidths at -10 dB wider than 5 GHz and reflection coefficients below -5 dB over the whole frequency range from 8 up to 18 GHz. To this purpose, we apply the modeling approach described in Section II, assuming a resonant frequency $f_{\rm r} = 13$ GHz, i.e., the median value between 8 and 18 GHz.

From data reported in Fig. 7(b), it results that at 13 GHz, the coatings filled at 9% wt, at 10% wt, and at 13% wt of GNPs have an average effective electrical conductivity value of 26.7 S/m, 29.6 S/m, and 38.26 S/m, respectively. For such conductivities, the condition of perfect wave matching (11) requires that the thickness t of lossy sheets made of graphene-based coatings filled with GNPs at 9% wt, 10% wt, and 13% wt is equal to 99 μm, 90 μm, and 69 μm, respectively. Therefore, the coating loaded with 13% wt GNPs should be preferable, since it requires a thinner coating, i.e., a lower amount of material. However, when the GNP concentration increases there are some technological constrains since more agglomerates will appear [40] leading to a small increase of the PVDF/GNP electrical conductivity along with significant disadvantages in production process. Specifically, the functionalization of felt textiles with coatings having a GNP concentration higher than 10% wt gives rise to several inhomogeneities and nonuniformities due to difficulties in DMF removal during the curing process in the oven. As a consequence, the EM absorption is not uniform and the risk of coating removal during the production process or use is higher. Thus, we decided to limit the GNP concentration to 10% wt GNPs.

Furthermore, a compromise is needed in the coating thickness selection. In fact, even though the ideal thickness would be around 90 μm, we observed that such thickness value undermines the uniformity of the coating, the GNP dispersion in the polymer matrix, leading to poor EM properties. Therefore, we limited the maximum coating thickness up to 70 μm and, considering technological constraints in the production process, we selected two target values for the thickness: 60 μm and 70 μm.

On the other hand, the functionalization of polyester fabrics is less challenging since the fabric surface is smoother. Hence, in order to reduce the coating thickness, we selected a 13% wt loaded PVDF/GNP coating. Also in this case, we select a thickness lower than the optimal value in order to avoid any handling-related issues and to limit the inhomogeneities and nonuniformities due to the higher GNP content.

The spacer thickness $d_{\rm S}$ is then computed by implementing an iterative procedure aimed at minimizing the value of the

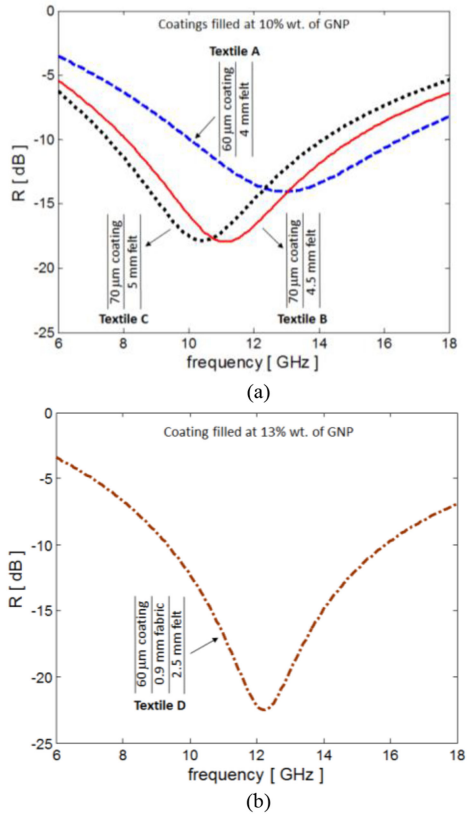

Fig. 8. Calculated reflection coefficients of (a) textiles A, B, and C, and (b) textile D.

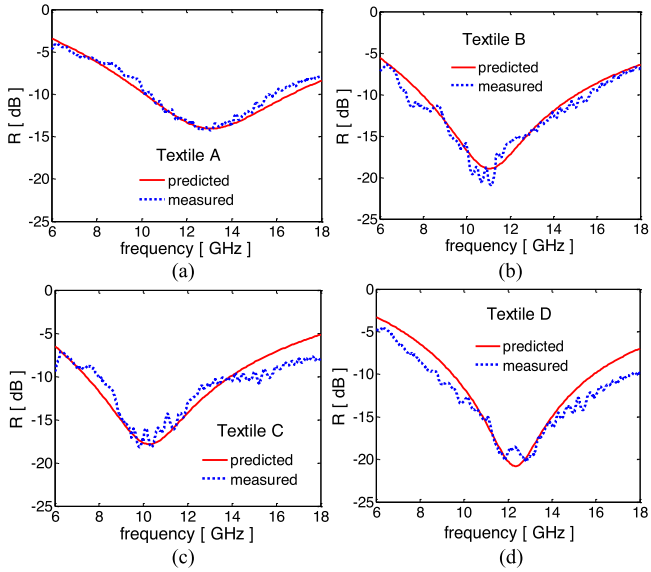

Fig. 9. Reflection coefficient versus frequency of the predicted and fabricated textiles: (a) A, (b) B, (c) C, and (d) D having the configurations reported in Fig. 9(a) and (b).

reflection coefficient R in (7) [32] and taking into account that commercially available polyester felts have thicknesses ranging between 2 and 5 mm. In particular, we designed four absorbing textiles, namely A, B, C, and D.

Textile A is made with a 60 μm-thick PVDF/GNP coating over a commercial 4 mm-thick polyester felt, whereas textiles B and C include 70 μm-thick PVDF/GNP coating over commercial polyester felts having thickness equal to 4.5 and 5 mm, respectively. Coatings over textiles A, B, and C are filled at 10% wt of GNPs.

Finally, textile D consists of a 60 μm-thick PVDF/GNP coating filled at 13% wt and cast over a 0.9 mm-thick polyester woven fabric and attached to a 2.5 mm-thick polyester felt. Fig. 8 shows the computed reflection coefficients spectra of the resulting configurations of absorbing textiles A, B, C [see Fig. 8(a)], and D [see Fig. 8(b)]. In the same figures, the textile configurations are summarized and sketched.

E. Reflection Coefficient of Graphene Based Absorbing Textiles

The reflection coefficients of the produced graphene absorbing textiles are measured in the frequency range from 8 to 18 GHz as described in Section II.

The frequency spectra of the measured and predicted reflection coefficients are reported in Fig. 9(a)–(d) for textiles A, B, C, and D, respectively. The measured data show ripples due to panel edge scattering and environmental EM noise, since measurements are performed in free-space.

It is worth to notice that all the produced wideband absorbing textiles fully satisfy the design requirements, since they all have bandwidths at -10 dB wider than 5 GHz and reflection coefficient below -5 dB over the entire frequency range from 8 to 18 GHz. Then, in all cases there is a good agreement between the spectra of measured and predicted reflection coefficients. In particular, the best agreement between measured and computed data is achieved for textile A, since it includes a coating filled with only 10% wt GNPs and with thickness limited to 60 μm. In fact, as discussed in previous Sections, this coating is characterized by a better uniformity of the filler distribution and by a reduced amount of local filler agglomerations. Also textile D has a 60 μm-thick coating made with 13% wt. GNPs, which is characterized by a higher density of imperfections and inhomogeneities that originates oscillations in the measured spectrum of the reflection coefficient.

On the other hand, textile C, including a 70 μm-thick coating, is characterized by a measured reflection coefficient affected by a higher degree of noise, since the coating is less uniform with respect to the coatings of textiles A and B. However, there is a good agreement with the expected EM performance and the obtained absorber shows a wider bandwidth than textile A. Finally, in case of textile D the ripples are mainly due to air gaps between the felt layer and the woven fabric.

All of the produced graphene-based absorbing textiles show a reflection coefficient with a bandwidths Δf at -10 dB ranging between 5.2 and 8.6 GHz, as reported in Table II in terms of percentage value of the resonant frequency f_{r}. In particular, textiles B, C, and D, including a thicker coating or a higher GNP amount, have a wider band at -10 dB, since the coating conductivity σ is closer to the ideal lossy sheet conductivity σ_{L} given by the perfect wave matching condition (11).

TABLE II
SHEET RESISTANCE AND DC ELECTRICAL CONDUCTIVITY OF THE PRODUCED PVDF/GNP COATED TEXTILES

Textile	f_r [GHz]	Δf [%]
A	13	40
B	11	77
C	10	60
D	12	72

IV. CONCLUSION

In this article, different graphene-based wideband absorbing textiles are designed, produced, and characterized. They all satisfy the design condition of reflection coefficient below −5 dB over the 8–18 GHz frequency range and show frequency bandwidths at −10 dB ranging between 40% and 77% of their corresponding resonant frequency. Moreover, such coating textiles are low-weight, cost-effective and can be easily handled without risk of damaging the coating. In addition, they are found to be super-hydrophobic, and hence believed to be washable without properties' degradation and capable of resisting long-term real world exposure and industrial contamination tests.

The realization of these graphene-based absorbing textiles required the development of a new production process of PVDF/GNP coatings suitable to be cast directly over commercial textiles.

All the produced coated textiles are characterized in terms of morphological, electrical, and EM properties. In particular, an innovative technique was used for the EM characterization of all the produced coatings. At first, the complex permittivity of a benchmark sample is measured, then the average size of GNPs is estimated and used to predict the effective complex permittivity of graphene-based coatings loaded with different GNP amounts by means of the MG model. Such predictions are used to design radar absorbing textiles with reflection coefficients below −5 dB over the frequency range from 8 up to 18 GHz. These textiles are then produced and are demonstrated to fully satisfy the requirements, showing also a reflection coefficient with a bandwidth at −10 dB ranging between 40% and 77% of their resonant frequency.

ACKNOWLEDGMENT

The authors would like to thank Prof. Alessio Tamburrano for technical support during EM characterization and for technical discussions.

REFERENCES

[1] C. Christopoulos, "Electromagnetic compatibility (EMC) in challenging environments," *Oper. Res., Eng., Cyber Secur.*, vol. 113, pp. 95–115, 2017.

[2] J. Liu *et al.*, "Microwave absorption enhancement of multifunctional composite microspheres with spinel Fe_3O_4 cores and anatase TiO_2 shells," *Small*, vol. 8, no. 8, pp. 1214–1221, Feb. 2012.

[3] A. Namai *et al.*, "Synthesis of an electromagnetic wave absorber for high-speed wireless communication," *J. Amer. Chem. Soc.*, vol. 131, no. 3, pp. 1170–1173, Dec. 2008.

[4] P. DeRoy *et al.*, "Effectiveness of noise suppressing sheet material for mitigation of automotive radiated emissions," *IEEE Trans. Electromagn. Compat.*, vol. 63, no. 2, pp. 398–409, Apr. 2021.

[5] C. A. Stergiou, M. Y. Koledintseva, and K. N. Rozanov, "Hybrid polymer composites for electromagnetic absorption in electronic industry," in *Hybrid Polymer Composite Materials*. Sawston, U.K.: Woodhead Publishing, 2017, pp. 53–106.

[6] F. Bilotti, A. Toscano, K. B. Alici, E. Ozbay, and L. Vegni, "Design of miniaturized narrowband absorbers based on resonant-magnetic inclusions," *IEEE Trans. Electromagn. Compat.*, vol. 53, no. 1, pp. 63–72, Feb. 2011.

[7] P. Kaur, S. Bahel, and S. B. Narang, "Microwave absorption behavior and electromagnetic properties of Ni-Zr doped La-Sr hexagonal ferrite synthesized by auto-combustion method," *Mater. Res. Bull.*, vol. 100, pp. 275–281, Apr. 2018.

[8] D. Micheli *et al.*, "Reduction of satellite electromagnetic scattering by carbon nanostructured multilayers," *Acta Astronautica*, vol. 88, pp. 61–73, Jul. 2013.

[9] H.-T. Chou and Y.-S. Chang, "Statistical analysis of fabrication discrepancy effects on periodic circuit analog electromagnetic absorbers," *IEEE Trans. Electromagn. Compat.*, vol. 63, no. 2, pp. 410–418, Apr. 2021.

[10] V. K. Chakradhary, H. B. Baskey, R. Roshan, A. Pathik, and M. J. Akhtar, "Design of frequency selective surface-based hybrid nanocomposite absorber for stealth applications," *IEEE Trans. Microw. Theory Techn.*, vol. 66, no. 11, pp. 4737–4744, Nov. 2018.

[11] H. B. Baskey, E. Johari, and M. J. Akhtar, "Metamaterial structure integrated with a dielectric absorber for wideband reduction of antennas radar cross section," *IEEE Trans. Electromagn. Compat.*, vol. 59, no. 4, pp. 1060–1069, Aug. 2017.

[12] J. Ma *et al.*, "Systematic study of microwave absorption, heating, and microstructure evolution of porous copper powder metal compacts," *J. App. Phys.*, vol. 101, no. 074906, pp. 1–8, Apr. 2007.

[13] S. Padhy, A. De, R. R. Debata, and R. S. Meena, "Design, characterization, and optimization of a multilayer U-type hexaferrite-based broadband microwave absorber," *IEEE Trans. Electromagn. Compat.*, vol. 60, no. 6, pp. 1734–1742, Dec. 2018.

[14] X. Liu *et al.*, "The microstructure of SiCN ceramics and their excellent electromagnetic wave absorbing properties," *Ceramics Int.*, vol. 41, no. 9, pp. 11372–11378, Nov. 2015.

[15] W. Liu *et al.*, "Fabrication of ultralight three-dimensional graphene networks with strong electromagnetic wave absorption properties," *J. Mater. Chem. A*, vol. 3, no. 7, pp. 3739–3747, Jan. 2015.

[16] M. M. Tirkey and N. Gupta, "Electromagnetic absorber design challenges," *IEEE EMC Mag.*, vol. 8, no. 1, pp. 59–65, Apr. 2019.

[17] G. Mittal *et al.*, "A review on carbon nanotubes and graphene as fillers in reinforced polymer nanocomposites," *J. Ind. Eng. Chem.*, vol. 21, pp. 11–25, Jan. 2015.

[18] M. Esen, I. İlhan, M. Karaaslan, and R. Esen, "Investigation of electromagnetic and ultraviolet properties of nano-metal-coated textile surfaces," *Appl. Nanoscience*, vol. 10, no. 2, pp. 551–561, Jan. 2020.

[19] M. M. Bait-Suwailam, S. A. Thamer, and A. Akram, "A wearable reconfigurable electromagnetic metamaterial absorber using artificial magnetic inclusions," in *Proc. IEEE Int. Symp. Antennas Propag. USNC-URSI Radio Sci. Meeting*, Jul. 2019, pp. 1623–1624.

[20] M. Subhankar and A. Chatterjee, "Conductive polymer-based electroconductive textile composites for electromagnetic interference shielding: A review," *J. Ind. Textiles*, vol. 47, no. 8, pp. 2228–2252, 2018.

[21] Y. K. Hong *et al.*, "Electromagnetic interference shielding characteristics of fabric complexes coated with conductive polypyrrole and thermally evaporated AG," *Curr. Appl. Phys.*, vol. 1, no. 6, pp. 439–442, Dec. 2001.

[22] A. Kaynak and R. Foitzik, "Methods of coating textiles with soluble conducting polymers," *Res. J. Textile Apparel*, vol. 15, pp. 107–113, May 2011.

[23] V. Šafářová and M. Jiří, "Multifunctional metal composite textile shields against electromagnetic radiation—Effect of various parameters on electromagnetic shielding effectiveness," *Polym. Composites*, vol. 38, no. 2, pp. 309–323, May 2017.

[24] H. C. Bidsorkhi *et al.*, "3D Porous graphene based aerogel for electromagnetic applications," *Sci. Rep.*, vol. 9, no. 1, pp. 1–11, Oct. 2019.

[25] S. Lee *et al.*, "Smart contact lenses with graphene coating for electromagnetic interference shielding and dehydration protection," *ACS Nano*, vol. 11, no. 6, pp. 5318–5324, Feb. 2017.

[26] J. Chen, J. Wu, H. Ge, D. Zhao, C. Liu, and X. Hong, "Reduced graphene oxide deposited carbon fiber reinforced polymer composites for electromagnetic interference shielding," *Composites Part A, Appl. Sci. Manuf.*, vol. 82, pp. 141–150, Mar. 2016.

[27] A. G. D'Aloia, H. C. Bidsorkhi, A. Tamburrano, G. De Bellis, and M. S. Sarto, "PVDF-Graphene nanocomposite coatings for electromagnetic wave absorption," in *Proc. IEEE Int. Symp. Electromagn. Compat., Signal Power Integrity*, Jul. 2019, pp. 90–94.
[28] H. C. Bidsorkhi *et al.*, "Nucleation effect of unmodified graphene nanoplatelets on PVDF/GNP film composites," *Mater. Today Commun.*, vol. 11, pp. 163–173, Jun. 2017.
[29] G. S. Wang *et al.*, "Fabrication of reduced graphene oxide (RGO)/Co_3O_4 nanohybrid particles and a RGO/Co_3O_4/Poly (vinylidene fluoride) composite with enhanced wave-absorption properties," *ChemPlusChem*, vol. 79, no. 3, pp. 375–381, Mar. 2014.
[30] H. C. Bidsorkhi *et al.*, "Flexible graphene based polimeric electrodes for low energy applications," in *Proc. 2020 IEEE Int. Symp. Nanotechnol.*, Jul. 2020, pp. 263–266.
[31] F. Geyer *et al.*, "When and how self-cleaning of superhydrophobic surfaces works," *Sci. Adv.*, vol. 6, Jan. 2020, Art. no. 3.
[32] A. G. D'Aloia, F. Marra, A. Tamburrano, G. De Bellis, and M. S. Sarto, "Electromagnetic absorbing properties of graphene–polymer composite shields," *Carbon*, vol. 73, pp. 175–184, Jul. 2014.
[33] A. Rinaldi, A. Proietti, A. Tamburrano, and M. S. Sarto, "Graphene-coated honeycomb for broadband lightweight absorbers," *IEEE Trans. Electromagn. Compat.*, vol. 60, no. 5, pp. 1454–1462, Oct. 2018.
[34] G. Spinelli *et al.*, "Dielectric spectroscopy and thermal properties of poly (lactic) acid reinforced with carbon-based particles: Experimental study and design theory," *Polymers*, vol. 12, no. 10, pp. 1–25, Sep. 2020.
[35] E. Li *et al.*, "Multifunctional and superhydrophobic cellulose composite paper for electromagnetic shielding, hydraulic triboelectric nanogenerator and joule heating applications," *Chem. Eng. J.*, vol. 420, Sep. 2021, Art. no. 129864.
[36] L. C. Jia *et al.*, "Robustly superhydrophobic conductive textile for efficient electromagnetic interference shielding," *ACS Appl. Mater. Interfaces*, vol. 11, no. 1, pp. 1680–1688, 2018.
[37] M. S. Sarto, A. G. D'Aloia, A. Tamburrano, and G. De Bellis, "Synthesis, modeling, and experimental characterization of graphite nanoplatelet-based composites for EMC applications," *IEEE Trans. Electromagn. Compat.*, vol. 54, no. 1, pp. 17–27, Feb. 2012.
[38] J. Lesnikowski, "Dielectric permittivity measurement methods of textile substrate of textile transmission lines," *Przeglad Elektrotechniczny*, vol. 3, pp. 148–151, Nov. 2012.
[39] M. G. Buonomenna *et al.*, "Poly (vinylidene fluoride) membranes by phase inversion: The role the casting and coagulation conditions play in their morphology, crystalline structure and properties," *Eur. Polym. J.*, vol. 43, no. 4, pp. 1557–1572, Apr. 2007.
[40] A. Tamburrano, F. Marra, J. Lecini, and M. S. Sarto, "Complex permittivity extraction method of a thin coating: EM properties of a graphene-based film on a composite layer," in *Proc. IEEE Int. Symp. EMC Eur.*, Aug. 2018, pp. 602–607.
[41] F. Marra *et al.*, "Electromagnetic and dynamic mechanical properties of epoxy and vinylester-based composites filled with graphene nanoplatelets," *Polymers*, vol. 8, no. 8, pp. 1–18, Aug. 2016.
[42] K. J. Vinoy and R. M. Jha, *Radar Absorbing materials—From Theory to Design and Characterization*, Boston, MA, USA: Kluwer Academic Publishers, 1996.
[43] K. N. Rozanov and M. Y. Koledintseva, "Matching conditions for a homogeneous absorbing layer," in *Procedia Engineering*. Amsterdam, The Netherlands: Elsevier, vol. 216, pp. 79–84, Jul. 2017.

Alessandro Giuseppe D'Aloia (Member, IEEE) received the bachelor's degree in materials engineering from the University of Perugia, Perugia, Italy, in 2007, and the master's and Ph.D. degrees in electrical engineering from the Sapienza University of Rome, Rome, Italy, in 2009 and 2014, respectively.

He is currently an Assistant Professor with the Sapienza University of Rome. His research interests include the development and the electromagnetic modeling of new graphene-based nanocomposites and nanostructerd materials for electromagnetic compatibility and sensing applications.

Hossein Cheraghi Bidsorkhi (Member, IEEE) received the bachelor's degree in polymer engineering from Azad University, Isfahan, Iran, in 2009, and the M.S. degree in polymer technology from the University Technology Malaysia, Johor, Malaysia, in 2013 and the Ph.D. degree in electrical, material and nanotechnology engineering from the Sapienza University of Rome, Rome, Italy, in 2018.

He is currently a Senior Research Fellow in material and nanotechnology engineering with the Sapienza University of Rome. He has pioneered research in developing advanced polymer nanocomposites for several applications, including smart textile, sensing, electrical, electromagnetic, energy harvesting, biomedical, drug delivery, and healthcare. He has been the Principal Investigator of several research projects.

Giovanni De Bellis (Member, IEEE) received both the Laurea degree in materials engineering and the Ph.D. degree in electrical engineering (scholarship in Nanotechnology), from the University of Rome "Sapienza", Rome, Italy.

He is currently serving as an Associate Professor with Sapienza University of Rome. His research activity is mainly focused on the development of polymer nanocomposites for applications in EMI shielding, RAMs, strain sensors, sweat, and humidity sensors. More recently, he became interested in soft electrostatic actuators as well as in novel methods for the measurement of the static dielectric permittivity. He has authored and coauthored more than 70 scientific publications, including several patents, and is an Editorial Board Member of the scientific journals *Heliyon* and *Electronic Materials*. He has been a member of IEEE since 2012.

Maria Sabrina Sarto (Fellow, IEEE) received the Laurea, summa cum laude and the Ph.D. degrees in electrical engineering from the University of Rome Sapienza, Rome, Italy, in 1992 and 1997, respectively.

Since 2005, she has been a Full Professor of electrotechnics and electromagnetic compatibility with the Faculty of Engineering, Sapienza University, Rome, Italy, where she has been Deputy Rector for Research since 2020, Deputy Rector for Research Infrastructures and Tools from 2014 to 2020, Director of the Department of Astronautical, Electrical and Energy Engineering since 2016, Director of the Research Center on Nanotechnology Applied to Engineering of Sapienza from 2006 to 2015, Director of the Electromagnetic Compatibility Laboratory at the Department of Electrical Engineering since 1998, and Director of the Nanotechnology and Nanoscience Laboratory of Sapienza University from 2010 to 2015. She has authored or coauthored more than 210 papers in the fields of electromagnetic compatibility (EMC), advanced materials for EMC, graphene-based materials for EM shielding and absorption, and for sensing.

Prof. Sarto was Distinguished Lecturer of the IEEE EMC Society in 2001–2002. She has been Associate Editor of IEEE EMC-T (1998-2018), Co-Chair of the IEEE EMC Society TC11 on "Nanotechnology and Advanced Materials", member of the Advisory Board of the IEEE Council on Nanotechnology, Chair of the working group IEEE STD 299.1 of IEEE EMC Society, Co-Chair of IEEE NANO 2015 and of EMC Europe 2020. She was recipient of several awards from the IEEE EMC Society and the Society of Automotive Engineers.